GDCh

Research Articles

Angewandte
Chemie
International Edition
www.angewandte.org

Reaction Mechanisms | Hot Paper

Brønsted Acid Catalysis—Controlling the Competition between Monomeric versus Dimeric Reaction Pathways Enhances Stereoselectivities

Maximilian Franta, Johannes Gramüller, Philipp Dullinger, Simon Kaltenberger, Dominik Horinek, and Ruth M. Gschwind*

Abstract: Chiral phosphoric acids (CPA) have become a privileged catalyst type in organocatalysis, but the selection of the optimum catalyst is still challenging. So far hidden competing reaction pathways may limit the maximum stereoselectivities and the potential of prediction models. In CPA-catalyzed transfer hydrogenation of imines, we identified for many systems two reaction pathways with inverse stereoselectivity, featuring as active catalyst either one CPA or a hydrogen bond bridged dimer. NMR measurements and DFT calculations revealed the dimeric intermediate and a stronger substrate activation via cooperativity. Both pathways are separable: Low temperatures and high catalysts loadings favor the dimeric pathway (*ee* up to −98 %), while low temperatures with reduced catalyst loading favor the monomeric pathway and give significantly enhanced *ee* (92–99 % *ee*; prior 68–86 % at higher temperatures). Thus, a broad impact is expected on CPA catalysis regarding reaction optimization and prediction.

Introduction

Brønsted acid catalysis has become one of the central pillars in organocatalysis over the last decades due to its huge potential and versatility in organic asymmetric synthesis.[1–5] BINOL (1,1′-bi-2-naphthol) derived chiral phosphoric acids (CPAs) emerged as one of the most famous catalyst types in this field. After their initial report by Akiyama[6] and

[*] M. Franta, J. Gramüller, S. Kaltenberger, Prof. Dr. R. M. Gschwind
Institute of Organic Chemistry, University of Regensburg
Universitätsstraße 31, 93053 Regensburg (Germany)
E-mail: ruth.gschwind@chemie.uni-regensburg.de

P. Dullinger, Prof. Dr. D. Horinek
Department of Physical and Theoretical Chemistry, University of Regensburg
Universitätsstraße 31, 93053 Regensburg (Germany)

Terada,[7] various CPAs with different 3,3′-substituents were introduced by several groups[8–10] and adapted to a myriad of transformations.[11–19]

From these reactions, the transfer hydrogenation of imines with Hantzsch Ester (HE) was later established as model system for mechanistic investigations (see Figure 1A). NMR measurements were key to investigate and assess the hydrogen bond assisted ion-pair CPA/imine intermediates. These experimental investigations allowed a better understanding of the reaction mechanisms by revealing transition states,[20] structures[21–23] and hydrogen bond strengths.[24,25] In our NMR studies we detected intermediates with one or two catalyst molecules.[25–27] Furthermore, Niemeyer et al. revealed that supramolecularly linked CPAs show cooperativity effects in the transformation of quinolines.[26] This raised the question, whether competing monomeric and dimeric reaction pathways may be a general feature in catalytic reactions with CPAs or even in Brønsted acid catalysis. In case monomeric and dimeric pathways provide different enantioselectivities, guidelines to switch on and off one of the pathways would allow to improve synthetic applications and mechanistic studies.

Besides experimental and spectroscopic investigations, computational studies have been key to a deeper understanding of the reactivity and stereoselectivity of CPA-catalyzed reactions.[28,29] Goodman et al. linked the stereoselectivity to two parameters reflecting the steric properties of the 3,3′-substituents and developed a model for predicting suitable CPAs based on reactant structures.[30,31] Independent studies of Sigman et al. established a data-driven prediction model to elucidate the influence of multiple parameters of the reagents on the stereoselectivity.[32–34] Nevertheless, despite the ground-breaking achievements of computations,[35] NMR measurements and other methods,[36] a simple and easy prediction of the optimal catalyst for each substrate/reagent combination remains still extremely challenging.

A potential explanation for the observed complexity of effects might be the overlooked competition of monomeric and dimeric pathways mentioned above. Niemeyer et al. discovered such a competing reaction pathway featuring a hydrogen bond bridged dimeric CPA species for the transfer hydrogenation of quinolines using interlocked CPAs and **1d** as catalysts (see Figure 1B).[26] In general a very low population of dimeric CPA/CPA/substrate intermediates is expected. However, the observed stereoselectivity/catalyst

Angew. Chem. Int. Ed. **2023**, *62*, e202301183 (1 of 9)

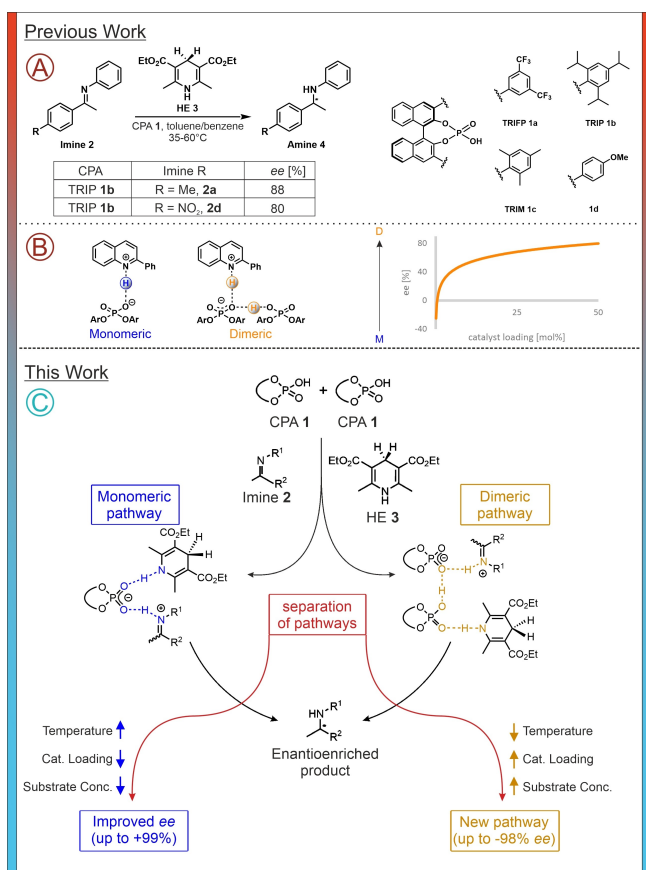© 2023 The Authors. Angewandte Chemie International Edition published by Wiley-VCH GmbH

Figure 1. A) Previously optimized CPA-catalyzed transfer hydrogenation of imines. At a temperature range of 35–60 °C, stereoselectivities of 80 to 93 % were achieved B) Monomeric CPA/substrate and dimeric CPA/CPA/substrate intermediates observed in our previous work with Niemeyer.[25] The competition of monomeric and dimeric reaction channel led to a strong dependence of stereoselectivity on the catalyst loading. C) Separation of monomeric and dimeric reaction pathway in the CPA-catalyzed transfer hydrogenation of imines via modulation of the reaction conditions (temperature, catalyst loading, substrate conc.) allowed to further optimize stereoselectivities. In this work, we present a way to improve the stereoselectivity of the CPA-catalyzed transfer hydrogenation of imines by considering the influence of the dimeric pathway. This allows us to separate both pathways, which leads to an improvement of stereoselectivity for the classic monomeric pathway as well as the establishment of a second route to obtain high enantioselectivities via the dimeric pathway.

loading correlation revealed that the dimeric pathway leads to an inversion of the enantiomeric excess (*ee*) even at catalyst loadings <10 mol % typical for organocatalysis.[26] The minimal concentration of CPA/CPA/quinoline intermediates was additionally corroborated by our NMR investigations. The specific hydrogen bond pattern in the ^{1}H NMR spectra could be only detected at a CPA quinoline ratio of 2:1. To explain the strong effect of CPA/CPA/quinoline complex on the catalytic outcome, the tiny concentration must be overcompensated by a strong kinetic preference of the dimeric pathway. Indeed, the respective DFT calculations of the twofold transfer hydrogenation of quinolines showed a kinetic dominance of the dimeric species in the stereoselective second reduction step.[26,37]

Therefore, the dimeric pathway can take over the stereoselectivity of the reaction despite a very low population of the CPA/CPA/quinoline intermediate at <10 mol % catalyst loading. This observation raises the question, whether the dominance of the dimeric pathway is an exception for quinolines and catalysts with moderate steric hindrance or whether it is a general feature of CPA-catalyzed reactions. Hence, separating monomeric and dimeric reaction pathway and optimizing each one specifically could open up new possibilities to improve the stereoselectivity of not only this reaction but many CPA-catalyzed reactions in general.

Therefore, in this study, we investigated the competition between monomeric and dimeric pathway in the CPA-catalyzed transfer hydrogenation of imines. A screening of 7 CPAs and 13 imines with NMR spectroscopy and/or determination of enantiomeric excess by chiral HPLC revealed a high impact of the dimeric pathway on the *ee* in all tested reactions. Steric and electronic influences of both CPA and imine substituents on the dimer formation were investigated. In addition, reaction conditions were screened and adjusted to separate monomeric and dimeric pathways (see Figure 1C). This was key to significantly improve stereoselectivities for the monomeric as well as the dimeric pathway.

Results and Discussion

Model systems: In order to check, whether 2:1 CPA/CPA/ imine intermediates (further referred to as dimers) are a general feature in CPA catalysis we selected as model systems the most commonly used CPAs[1] TRIFP **1a** (3,3′-bis(3,5-bis (trifluoromethyl)phenyl)-1,1′-binaphthyl-2,2′diyl hydrogen phosphate),[10,38] TRIP **1b** (3,3′-bis(2,4,6-triisopropylphenyl)-1,1′-binaphthyl-2,2′diyl hydrogen phosphate),[8] TRIM **1c** (3,3′-bis(2,4,6-trimethylphenyl)-1,1′-binaphthyl-2,2′diyl hydrogen phosphate) and TiPSY **1e** (3,3′-bis(triphenylsilyl)-1,1′-binaphthyl-2,2′diyl hydrogen phosphate)[39] as well as catalysts **1d**,**f**,**g** to probe the effects of varying steric and electronic properties (see Figure 2a). As substrates the imines **2a–2n** were chosen to test the influence of steric and electronic effects of the imine on the dimer formation (see Figure 2b).

NMR investigations on CPA/CPA/imine formation: To reveal the structure and mode of activation of the CPA/ CPA/imine intermediates as well as factors favoring their formation, we performed a detailed NMR spectroscopic study. Already trace amounts of the dimer intermediates below the NMR detection limit could significantly affect the stereoselectivity with quinolines, while the best experimental conditions to investigate the dimeric species via NMR spectroscopy were found to be a 2:1 ratio of catalyst to quinoline.[26,37] Therefore, also the NMR measurements for the CPA/imine combinations were conducted at a 2:1 ratio of catalyst and imine. Low temperature is the key to slow down exchange processes and to make the proton signals in the hydrogen bonds detectable, which are crucial for the differentiation of the monomeric and the dimeric
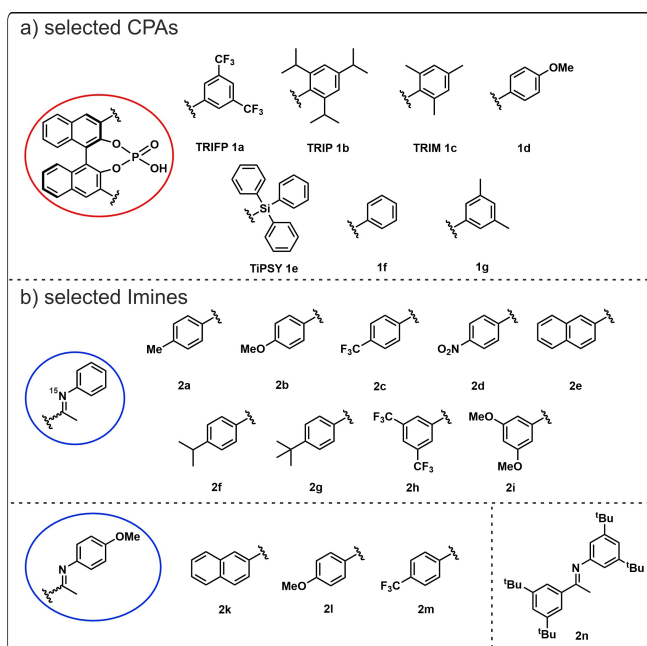
Figure 2. Structures of the investigated a) chiral phosphoric acids (CPAs) with different 3,3'-substituents and b) imines with different steric and electronic properties of the imine. A variety of combinations of these imines was investigated by NMR spectroscopy to elucidate trends of the dimer formation.

Figure 3. A) General hydrogen bond pattern observed for CPA/CPA/imine intermediates featuring PO⁻–H–N⁺ and PO–H–OP hydrogen bonds for the monomeric (blue) and dimeric (orange) complex. B) DFT structure models for the two different conformers of [**1a/1a**/*E*-**2b**] differing in the hydrogen bond situation and accessibility of the P=O hydrogen bond acceptor (see Supporting Information 3.6 for details). DFT calculations were performed on a TPSS/def2-SVP (def2/J) level of theory with implicit solvent (CPCM) and the D3BJ correction based on the previous DFT studies[37] and the observed NOE restraints (see Supporting Information 3.6 for details and references). C) ¹H NMR spectra of the systems TiPSY **1e**+**2b** (bottom), TRIFP **1a**+**2b** (middle) and Phenyl-CPA **1f**+**2b** (2:1 stoichiometry, 50 mM:25 mM, CD₂Cl₂, 180 K, 600 MHz) show the steric influence of the 3,3′-substituents on dimer formation: Bulky substituents favour the formation of the monomers, small substituents give monomers and dimers, while for TRIFP **1a** a general preference for dimer formation is observed.

intermediates.[22,26] Therefore, all NMR spectra were recorded in CD₂Cl₂ at −93 °C.

To our surprise we were able to clearly identify the 2:1 CPA/CPA/imine dimer for many CPA/imine combinations at these conditions[40] (see Supporting Information 3.4 and 6.1). In addition, for some systems we even obtained well resolved spectra with reasonable line widths, which allowed for the first time NOESY, HOESY and relaxation dispersion measurements for CPA/CPA/imine dimers (see Supporting Information 3.6). In the following, the NMR spectroscopic identification and characterization of the dimeric intermediate is exemplarily discussed for **1a/1a/2b**.

In the hydrogen bond region[22] of the ¹H-spectrum the characteristic pattern of four complexes can be identified. Most prominent is the H-bond signal pattern for dimeric **1a/1a/2b** with an *E*-configured imine while the respective dimeric complex with a *Z*-imine is by far less populated (see Figure 3A orange signals). Due to the ¹⁵N labelling of the imine (I(¹⁵N)=¹⁄₂), the PO⁻–H–N⁺ hydrogen bonds can be clearly identified via their doublet splitting, while the PO–H–OP hydrogen bonds of **1a/1a/2b** appear as singlets (both signals have a 1:1 integral ratio confirming the dimeric species). In addition, small amounts of the corresponding monomeric **1a/2b** species with both *E*- and *Z*-imine are observed (see Figure 3A blue signals). The assignment of *E*- and *Z*-configurations in the dimeric complexes was based on NOESY spectra and characteristic exchange peaks with the previously investigated monomeric **1a/2b** complexes.[21] Diffusion ordered spectroscopy (DOSY) measurements were performed and validated the assignment as dimeric
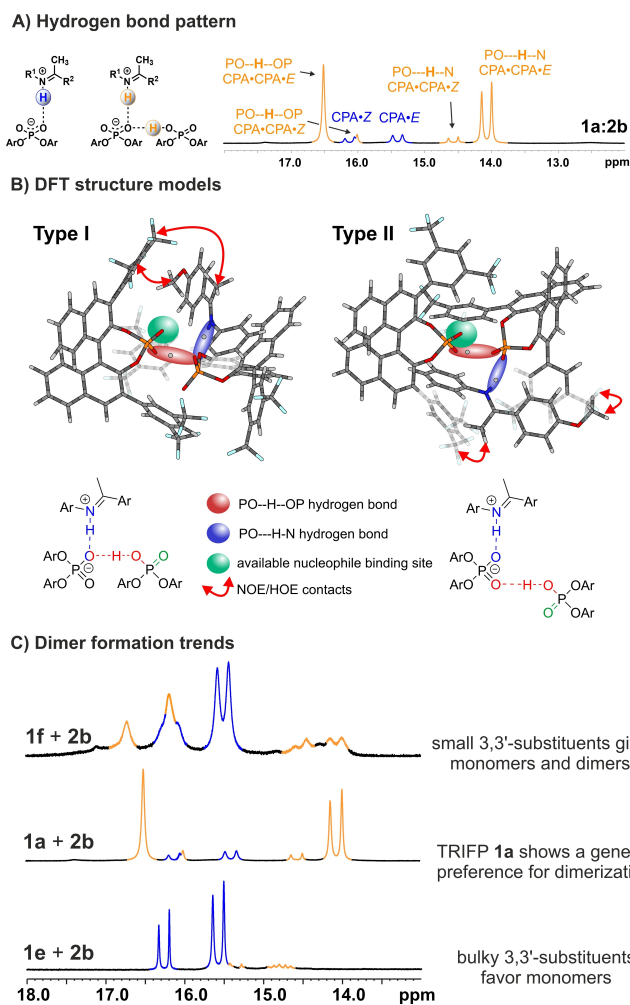
species (dimeric **1a/1a**/*E*-**2b** 3760±27 Å³; monomeric **1a**/*E*-**2b** 2150±36 Å³; for details see Supporting Information 3.5). ¹H, ¹H NOESY and ¹H, ¹⁹F HOESY studies were conducted to shed light onto the potential structure of **1a/1a**/*E*-**2b** (see Figure 3B and Supporting Information 3.6). Furthermore, DFT calculations were performed on a TPSS/def2-SVP (def2/J) level of theory with implicit solvent (CPCM) as well as a D3BJ correction based on the previous DFT studies[26,37] and the observed NOE restraints (see Supporting Informa-

tion 3.6 for details and references). Similar to the monomeric **1a**/**2b** complexes showing one set of signals for two conformations in fast exchange on the NMR time scale, also for this dimeric species two conformations Type I and Type II were found both matching the experimentally observed pattern of NOE/HOE contacts (see Figure 3B red arrows). DFT pointed towards Type II as the more stable one (see Supporting Information 3.6). Relaxation dispersion $R_{1\rho}$ measurements corroborated the presence of a fast exchange process potentially between Type I and Type II (for details see Supporting Information 3.6).[41] In structure Type I both hydrogen bonds are directed to one oxygen atom of the central phosphoric acid while in Type II two oxygen atoms of the central CPA are involved. Furthermore, Type I offers a nucleophile binding site close to the imine which hypothetically would lead to the correct inverse product selectivity for the dimeric pathway. In Type II a reorganization would be necessary to enable the hydride transfer (see Supporting Information 3.6 for detailed discussion). The presented structures show that in the dimeric complexes both catalyst molecules together create the stereoinductive environment for the downstream transformation. Future theoretical calculations of these demanding systems with many degrees of freedom may be able to reveal which of the many potential transition state pathways is most probably active. These transition states may differ in the stacking of imine and Hantzsch ester (nucleophilic attack from top or bottom), *E*- or *Z*-imine configuration or hydrogen bonding motif (both H-bonds to one or two oxygen atoms, see Figure 3B).

Next the hydrogen bond properties of dimeric versus monomeric complexes were analyzed based on their NMR parameters. Both ^{1}H and ^{15}N chemical shifts of the dimeric species are clearly high field shifted and the $^1J_{NH}$ coupling constants are increased compared to the monomeric complexes with the same imine configuration (see Supporting Information 3.4). As demonstrated in previous H-Bond studies,[24,25] this clearly reflects a stronger proton transfer onto the imine in the dimeric intermediate based on cooperativity effects introduced by the second PO–H–OP hydrogen bond.[42–44] As the proton transfer onto the substrate is directly linked to the substrate's electrophilicity/ activation towards nucleophilic attacks, this might contribute to the dimeric reaction channel being kinetically dominant even at low catalyst loadings (< 10 mol%). Overall the NMR investigations show that the CPA/CPA/imine dimer intermediates seem to be a self-assembled supramolecular version of List's IDPIs[45] or Gong's linked bisphosphoric acids[46] regarding the spatial confinement provided by two CPA units and the increased acidity. Additionally, the observed hydrogen bond cooperativity is a prime example of "Brønsted acid assisted Brønsted acid catalysis"[47,48] as also observed for other Brønsted acid or hydrogen bond catalysts[49–51] and is typical for enzyme catalysis.[52,53]

Next, we investigated, whether special structural features of the CPA and/or the imine favor the formation of the dimeric species. For this analysis, we used the characteristic signal pattern of the complexes in the hydrogen bond region. For TRIFP **1a** a general preference for dimer formation was observed for several imines (see Supporting Information 3.4), while for catalysts with bulkier 3,3′-substituents (TRIP **1b** and TiPSY **1e**) no preference for the respective dimeric species was detected (see Figure 3C and Supporting Information 3.4.1). For catalysts with smaller 3,3′-substituents (TRIM **1c**, **1d**, **1f**, **1g**) the CPA/CPA/imine dimers are populated but not the dominant species and additional hydrogen-bonded species were detected. In contrast, the steric properties of the imine had no significant influence on the dimer formation. Even for the extremely bulky imine **2n** featuring four *t*-butyl groups, dimer formation was still observed with TRIFP **1a** (see Supporting Information 3.4.1). For imines with electron-withdrawing substituents such as **2c** and **2d**, a variety of hydrogen-bonded species was detected. For electron-donating substituents of the imine the dimeric species was generally preferred (see Supporting Information 3.4.2). Remarkably, by combining electron-donating with electron-withdrawing groups on the 3,3′-substituents and the imine or the other way around (e.g. **1d**/ **2d** or **1a**/**2b**) a stronger preference for the dimeric species was observed (up to 95% dimeric species; for specific ratios see Supporting Information 3.4.2 and 3.4.3).

Thus, we were able to identify CPA/CPA/imine species for many CPA imine combinations as key intermediate for a dimeric reaction pathway. The general hydrogen bond pattern reveals a cooperativity effect of the PO–H–OP and PO$^-$–H–N$^+$ hydrogen bond resulting in a stronger proton transfer onto the substrate potentially contributing to the kinetic preference of the dimeric reaction pathway. For the first time NOESY/HOESY studies gave experimental insights into the dimer structure. Together with DFT calculations they indicate that both catalyst molecules are most probably responsible for the stereoinduction. For many CPA/imine combinations the dimeric species was detected. Especially TRIFP **1a** and combinations with donating and withdrawing electronic properties on catalyst and imine favor dimer formation.
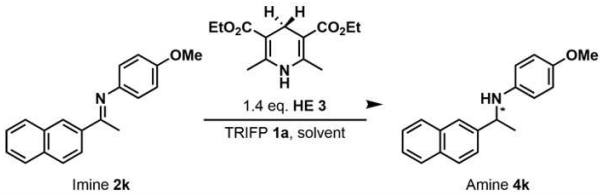
Probing the Participation of Dimeric Pathways: Next, we explored under which experimental conditions the dimeric reaction channel affects the actual catalysis. Then these results should be used to separate the two pathways, which potentially would improve stereoselectivity. In general, high overall concentrations, high catalyst loadings and sterically less hindered CPAs should favor the dimeric pathway. Furthermore, in case the activation barrier of the dimeric pathway is really lower also lower temperatures should favor the dimeric pathway.

First we checked, whether the dimeric pathway has any influence at previously optimized reaction conditions.[8,10] Based on our NMR screening and the fact that concentration effects were observed by Rueping et al.[10] we selected TRIFP **1a** and imine **2k**. The reaction was performed with varying catalyst loadings up to 40 mol% and the enantiomeric excess was determined by chiral HPLC. The reaction is considered irreversible without partial racemization of the product (see Supporting Information 4.1 for further discussion). In contrast to the transfer hydrogenation of quinolines which was investigated by Niemeyer et al.,[26] with our system no change in *ee* was observed upon

increasing the catalyst loading at 60 °C (see Supporting Information 4.1 Table S7). Hence, at higher temperatures exclusively the monomeric pathway seems to be active, which may also explain the elevated temperatures previously reported.[8, 10]

Next, multiple reaction conditions were adjusted and evaluated to reveal under which conditions the dimeric pathway is competing or even dominating. Therefore, enantioselectivities with varying catalyst loadings between 0.5 mol % and 20 mol % with (*R*)-TRIFP **1a** and imine **2k** were determined by chiral HPLC. Catalyst loadings of 0.5 mol % and 20 mol % (as typical upper limit in synthesis) were chosen as reference points for the monomeric and the dimeric pathway, respectively. In addition, different solvents and substrate concentrations were studied. First, benzene and toluene commonly used for this reaction as well as dichloromethane were compared. At 60 °C for benzene and toluene or 35 °C for dichloromethane (due to its lower boiling point) no significant differences in *ee* were observed between 0.5 mol % and 20 mol % catalyst loading (see Table 1—Entry 1–6). Only a slight effect of the absolute concentration between 0.03 mM and 0.06 mM was observed hinting at a potential slight contribution of the dimeric pathway at higher concentrations (see Table 1—Entry 3,4 versus Entry 7,8). However, by decreasing the reaction temperature to −10 °C a significant difference in *ee* was observed between 0.5 mol % and 20 mol % catalyst loading

for **2k** in both toluene and dichloromethane (see Table 1—Entry 9–12). While the Δ*ee* of both catalyst loadings in toluene is just 9 % (see Table 1—Entry 11,12), in dichloromethane a Δ*ee* of 30 % is observed (see Table 1—Entry 9,10). This indicates a significant impact of the dimeric pathway at higher catalyst loadings and reduced temperature.

These initial results clearly demonstrated that the high temperatures applied in previous reports effectively suppress the dimeric pathway, while lower temperatures support the dimeric pathway.

Optimization of stereoselectivity in the monomeric pathway: Under classical synthetic conditions (35–60 °C and 10–20 mol % catalyst loading)[8, 10] mainly the monomeric pathway is active (see above). Usually, lower temperatures provide improved stereoselectivities due to a better discrimination between the major and the minor enantiomer. However, in our system lowering the temperature should also support the dimeric pathway. Hence, the dimer contribution should change/decrease the stereoselectivity which would explain the high reaction temperatures reported previously.[8, 10] To counteract this contribution of the dimeric pathway at lower temperatures the catalyst loadings can be reduced. Therefore, the stereoselectivities of a variety of CPA/imine combinations were determined by chiral HPLC at different catalyst loadings (see Table 2). Imines **2a–e** and **2n** were selected to modulate electronic and steric properties and to allow a comparison with the NMR measurements (see Figure 2). Furthermore, dichloromethane was selected as solvent, as it showed the highest offset in *ee* values between high and low catalyst loadings (see Table 1). As initial test system TRIFP **1a** and imines **2a** and **2b** were chosen and the reaction was performed increasing the catalyst loadings stepwise from 0.1 mol % to 25 mol % at −10 °C (see Table 2). At 0.1 mol % catalyst

Table 1: Initial screening of reaction conditions to reveal a potential contribution of the dimeric pathway based on the *ee*. Catalyst loadings of 0.5 mol % and 20 mol % of (*R*)-TRIFP **1a** were chosen to shift the preference to the monomeric or dimeric pathway, respectively. Temperature and catalyst loading turned out to be key to differentiate between both pathways.

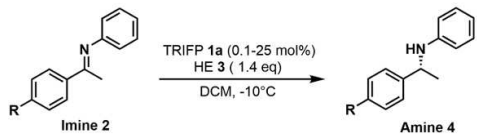| Entry	solvent	c [mM]	temp [°C]	cat.loading [%]	ee [%][c]
1	benzene	0.06	60	0.5	72
2	benzene	0.06	60	20	74
3	toluene	0.06	60	0.5	64
4	toluene	0.06	60	20	59
5	DCM	0.06	35	0.5	67
6	DCM	0.06	35	20	64
7	toluene	0.03	60	0.5	68
8	toluene	0.03	60	20	67
9	DCM	0.06	−10	0.5	73
10	DCM	0.06	−10	20	43
11	toluene	0.06	−10	0.5	68
12	toluene	0.06	−10	20	59

[a] Reaction was performed with 1.4 equiv HE **3** under Argon-atmosphere. [b] Enantiomeric excess was determined by HPLC using an IC column. [c] The absolute stereoconfiguration was determined based on analogy to prior reports.[9, 8, 10, 20]

Table 2: Tuning between monomeric and dimeric pathway using different catalyst loadings ((*R*)-TRIFP **1a** 0.1 mol % to 25 mol %) and the *ee* as mechanistic parameter.

Entry[a]	Cat. Loading [mol%]	ee 4a [%][b]	ee 4b [%][c]
1	0.1	99	99
2	5	48	-68
3	10	-5	-72
4	15	-50	-73
5	20	-62	-73
6	25	-98	-73

[a] Reaction was performed with imines **2a/b** and 1.4 equiv HE **3** under Argon-atmosphere. [b] Enantiomeric excess was determined by HPLC using an ODH column. [c] Enantiomeric excess was determined by chiral HPLC using an IA column.

loading an excellent *ee* value of 99% was reached for **4a** (Table 2—Entry 1), which is significantly higher than the 78% *ee* under previous conditions (60°C, benzene/toluene, 1–20 mol% **1a**).[10,21] At only 5 mol% of the CPA the *ee* value dropped drastically to 48% for **4a** and even inverted to −4% at 10 mol% catalyst loading. Using 25 mol% (*R*)-TRIFP **1a** for **4a** even led to an *ee* of −98%, which is again a strong increase in *ee* compared to the monomeric pathway with the opposite catalyst enantiomer ((*S*)-TRIFP (−78% *ee*, 60°C, benzene/toluene, 1–20 mol% **1a**). For **4b** also an increased *ee* value is observed at 0.1 mol%, but the inversion starts at lower catalyst loadings and is completely in the dimeric channel at 10 mol% catalyst. Thus, similar to the transfer hydrogenation of quinolines, also for imines the monomeric and the dimeric reaction channels lead to opposite enantiomers.
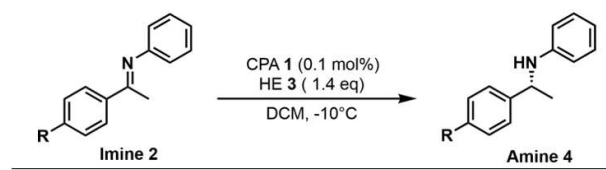
Overall the data in Table 2 indicates several points: 1.) The monomeric and the dimeric pathways can be separated at lower temperatures using adapted catalyst loadings. 2.) Significantly improved *ee* values over the monomeric pathway at high temperatures can be achieved via a combination of lower temperature and low catalyst loading. 3.) At lower temperatures the dimeric pathway is highly active at typical catalyst loadings reported previously.[10] 4.) Monomeric and dimeric reaction channel lead to opposite stereoselectivities providing different complexes and transition states (see above). 5.) By combining low temperature and high catalyst loading a complete inversion of the enantioselectivity can be achieved.

Next, the question arose whether in the optimized monomeric pathway improved *ee* values can be also obtained for other CPAs and imines. Hence, the reaction was performed with CPAs **1a–1d** and imines **2a–e** at −10°C with 0.1 mol% catalyst loading. Comparing the enantioselectivities achieved at 0.1 mol% catalyst loadings with *ee* values previously reported at higher temperatures[8,10,21] demonstrated the huge potential of the optimized monomeric pathway since in most of the tested cases we were able to improve the *ee* significantly (92–99% *ee* compared to 68–86% *ee* see Table 3). For TRIFP **1a** *ee* values above 95% were obtained with all imines tested and even for TRIP **1b**, which is most frequently used for this reaction, improved stereoselectivities could be obtained. At −10°C and 0.1 mol% catalyst loading for **1a/2b** 99% *ee* but lower yields were obtained (see Supporting Information 4.2, Table S10). However, reactions at 0°C and 0.5 mol% catalyst loading result in sufficient yields while maintaining higher stereoselectivities (95% *ee*; see Supporting Information 4.4) compared with previous conditions (72% *ee* at 60°C).[10]

In addition, concentration effects can be used as fine-tuning parameter for the *ee*. Low absolute concentrations (0.01 mM) favor the monomeric pathway and high absolute concentrations (0.06 mM) promote the dimeric pathway (see Supporting Information 4.4).

Optimization of stereoselectivity in the dimeric pathway: Next we evaluated the potential of the dimeric pathway for stereoselective transformations. To promote dimers, we combined increased catalyst loadings (20 mol%) with a

Table 3: Improved *ee* values applying the optimized reaction conditions for the monomeric channel. In comparison the *ee* values of previously reported reaction conditions are given. Especially for amines **4c** and **4d** significant improvements can be achieved.
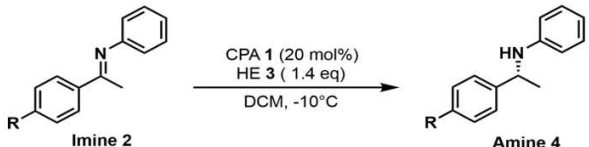

Entry[a]	CPA	Amine	*ee* [%][b]	Previous *ee* [%] with (*R*)-TRIP **1b**[c]/ (*R*)-TRIFP **1c**[d]
1	(*R*)-TRIFP **1a**	4a	99	86 / 78[e]
		4b	99	85 / 72[e]
		4c	98	84 / 70
		4d	99	81[e] / n.d.
2	(*R*)-TRIP **1b**	4c	96	84 / 70
3	(*R*)-TRIM **1c**	4c	96	84 / 70
		4d	96	81[e] / n.d.
4	(*R*)-**1d**	4c	95	84 / 70

[a] Reaction was performed with 0.1 mol% CPA **1**, 0.06 mM imine **2** and 1.4 equiv **3** under Argon-atmosphere at −10°C for 3 d. [b] Enantiomeric excess was determined by HPLC using an IA (**4b**, **4c**, **4d**, **4e**) and ODH (**4a**) column. [c] For comparison the *ee* values achievable with List et al.s reaction conditions with (*S*)-TRIP were used. (*R*)-TRIP and (*S*)-TRIP *ee* values are only inverted and then vary by up to 2%. Hence, a comparison with those values is possible to (*R*)-CPAs and the inverted *ee* values of List et al. are given.[8,20] [d] *ee* values achievable with Rueping et al.s reaction conditions with (*R*)-TRIFP.[10] [e] For the comparison of the *ee* of these ketimines, *ee* values with a PMP substituent on the aniline part of the ketimines were used. In general, a difference of up to 2% in *ee* can be observed between ketimines with and without the PMP substituent. Therefore, these were considered as eligible comparison values.[8,10,20]

reduced temperature (−10°C) for several (*R*)-CPAs (**1a–d**) and imines (**2a–e**, **2f**), as outlined in Table 4. For most of the systems an inversion of the *ee* was observed without significant reduction of the yield (see Supporting Information 4.4). Only imines with electron-withdrawing substituents (**2c**, **2d**) showed a significant decrease of *ee* instead of an inversion (see Table 4—Entry 3 excluding **1d** and Entry 4). These results reflect the trends in dimer formation detected in the NMR spectra that imines with electronegative substituents (**2c**, **2d**) disfavor dimers (see Supporting Information 3.4). Furthermore, the NMR spectra revealed that combining electron-donating and withdrawing substituents in the complex results in a preference for dimers. Again, this is directly reflected in the *ee*: for the combination **1d/2d** even for imines with electron-withdrawing substituents an inversion of the *ee* was observed (see Table 4—Entry 3 CPA **1d**).

This shows impressively that despite the concentration offset between NMR experiments and catalytic applications the trends in dimer formation can be consistently predicted. Even TRIP **1b**, which provides pronounced steric hindrance

Table 4: System screening to investigate the dimeric pathway at −10°C in DCM with 20 mol% catalyst loading. An inversion in *ee* can be observed with all systems except the ones with electron-withdrawing substituents at the aryl-ketone part of the ketimine (Entry **3**, **4**).

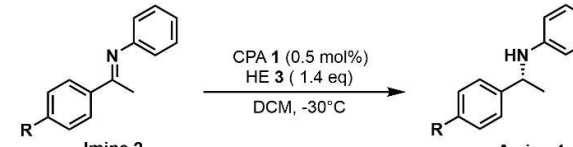| Entry[a]	Amine	CPA	*ee* [%][b]
1	**4a**	(R)-TRIFP **1a**	−98
		(R)-TRIM **1c**	−69
		(R)-**1d**	−73
2	**4b**	(R)-TRIFP **1a**	−73
3	**4c**	(R)-TRIP **1b**	30
		(R)-TRIM **1c**	30
		(R)-**1d**	−31
4	**4d**	(R)-TRIFP **1a**	72
		(R)-TRIM **1c**	44
5	**4e**	(R)-TRIFP **1a**	−86
		(R)-TRIP **1b**	−84
6	**4n**	(R)-TRIFP **1a**	−66
		(R)-TRIP **1b**	−98

[a] Reaction was performed with 20 mol% CPA **1**, 0.06 mM imine **2** and 1.4 equiv **3** under Argon-atmosphere at −10°C for 3 d. [b] Enantiomeric excess was determined by HPLC using an IA (**4b**, **4c**, **4d**, **4e**) and ODH (**4a**, **4n**) column.

Table 5: Setup optimization for the dimeric pathway. Cooling down the reaction to −30°C forces the reaction into the dimeric pathway with only 0.5 mol% catalyst loading. The *ee* of the monomeric pathway with the corresponding (S)-CPA can be improved using this setup.

Entry[a]	Amine	CPA	*ee* Dim.P. [%][b]	*ee* Mon.P. [%]
1	**4a**	(R)-TRIP **1b**	−92	−88
2	**4b**	(R)-TRIP **1b**	−95	−85
3	**4e**	(R)-TRIP **1b**	−98	−84

[a] Reaction was performed with 0.5 mol% CPA **1b**, 0.06 mM Imine **2** and 1.4 equiv **3** under Argon-atmosphere at −30°C for 6 d. [b] Enantiomeric excess was determined by HPLC using an IA (**4e**, **4b**) and ODH (**4a**) column.

of its 3,3′-substituents, showed an inversion proving a significant contribution of the dimeric pathway. Hence, the strong kinetic preference for the dimeric pathway can still be dominating despite very bulky CPAs and dimeric species below the NMR detection limit.

Finally, the inverted *ee* values from the dimeric pathway in Table 4 can be compared to those resulting from the monomeric pathway with the inverted catalyst enantiomer (inverted monomeric pathway at higher temperatures as previously reported[8,10,20]). Some of the values in Table 4 are already better or similar. However, to test the limits of both the dimeric and monomeric pathway optimization the temperature was further reduced to −30°C. Due to the strong kinetic preference of the dimeric pathway, at −30°C already 0.5 mol% catalyst loading was sufficient to force the reaction into the dimeric pathway (Table 5, for yields see Supporting Information 4.3). This also demonstrates the limitation of using low temperatures in the monomeric pathway.

Furthermore, the observed *ee* values of this setup were indeed above the reported *ee* values for the monomeric pathway with the inverted (S)-CPA. Again, the *ee* values could be improved to 92–98%. Hence, separating the pathways both, dimeric and monomeric pathway can be used to achieve excellent *ee* values.

Conclusion

Despite the great success of chiral phosphoric acids as privileged Brønsted acid organocatalysts and detailed mechanistic studies, an easy and general prediction of the optimal catalyst still remains challenging. In previous studies on a CPA-catalyzed transfer hydrogenation of quinolines, Niemeyer and coworkers[26] showed that in addition to the generally postulated monomeric pathway a dimeric pathway exists with opposite enantioselectivities. Here, we demonstrate that this dimeric pathway is active for a broad variety of CPAs typically used in the synthesis of chiral amines. Separating the monomeric and the dimeric pathway allowed to access significantly enhanced stereoselectivities for both product enantiomers.

Low temperature NMR measurements and DFT calculations shed light onto the structure of the hydrogen bond bridged CPA/CPA/imine dimer intermediates and their formation trends. Cooperativity effects of both catalysts—typical for ion-pair intermediates in apolar solvents—lead to a stronger substrate activation, which should result in a general kinetic preference of the dimeric reaction channel. In addition, cooperativity of both catalyst molecules leads to high potential stereoinduction. Hence, the supramolecular self-assembled dimer catalyst has similar features in terms of acidity/substrate activation and spatial confinement to the highly selective IDPi catalysts (and similar ones) developed by List and coworkers, in which two catalysts are fused by a covalent bond. A potential advantage of this self-assembly is the higher flexibility of the hydrogen bond compared to a covalent bond as linking unit, which may allow adaption to bulkier, more demanding systems. Due to the stronger substrate activation of the CPA/CPA dimer, the stereoselectivity of the transfer hydrogenation was found to be highly dependent on the contributions of monomeric and dimeric reaction pathway, which can be modulated by the reaction conditions (see Figure 4).
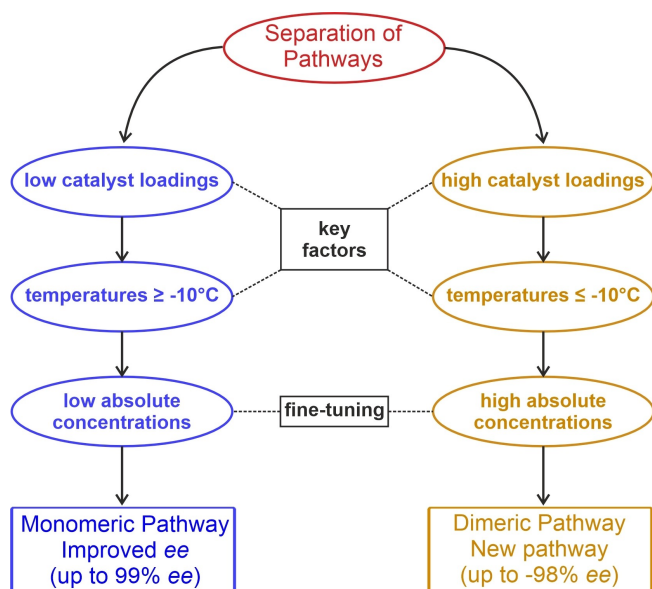
Figure 4. Separation of both reaction pathways by adjusting the reaction conditions. Catalyst loading and temperature play a key role to separate both pathways while the absolute concentration can be used for fine-tuning of *ee* and yield. In general, higher temperature, lower catalyst loadings and lower absolute concentrations can be used to force the reaction into the monomeric pathway. In contrast, lower temperatures, high catalyst loadings and high substrate concentrations are needed to force the reaction into the dimeric pathway.

In general, high temperatures (35–60 °C), low catalyst loadings (0.1–5 mol %) and lower concentrations favor the monomeric pathway, while low temperatures (−30 to −10 °C), high catalyst loadings (10–25 mol %) and higher concentrations favor the dimeric one. Both pathways were found to yield opposite enantiomers, leading to a reduction/ inversion of *ee* with increasing contribution of the dimeric pathway. Lowering the temperature (35–60 °C→−10 °C) while reducing the catalyst loading at the same time (10– 20 mol %→0.1 mol %) allowed us to stay in the monomeric channel and access higher *ee* values as prior at higher temperatures (here: 92–99 % *ee*; prior 68–86 % *ee*). This also gives one potential explanation why previous reactions were only performed at elevated temperatures. In addition, the *ee* inversion of the dimeric pathway is shown to provide the other product enantiomer with higher stereoselectivities than possible with the monomeric pathway at previously reported conditions (e.g. −98 % with the (R)-CPA dimeric pathway vs −84 % with the prior (S)-CPA monomeric pathway).

The kinetic preference of the dimeric pathway is nearly independent of the substrate and seems to be supported by the cooperativity effect between the two catalyst molecules. Therefore, the dimeric reaction channel is expected to contribute not only to the transfer hydrogenation of quinolines or imines, but to many other CPA-catalyzed reactions as well. We expect that the provided guidelines regarding temperature and catalyst concentrations to control the competition of monomeric and dimeric pathway can be transferred as a general Scheme. In addition, these insights may clarify otherwise confusing results (such as lower *ee* at lower temperature), open up new possibilities to further optimize stereoselectivities in Brønsted acid catalysis and lay the basis for refined mechanistic studies in experiment and theory.

Experimental Section

Synthesis of imines, HPLC data and chromatograms, NMR evaluation and spectra are given in the Supporting Information.

Conflict of Interest

The authors declare no conflict of interest.

Data Availability Statement

The data that support the findings of this study are available in the Supporting Information of this article.

[1] D. Parmar, E. Sugiono, S. Raja, M. Rueping, *Chem. Rev.* **2014**, *114*, 9047–9153.
[2] M. Terada, *Synthesis* **2010**, 1929–1982.
[3] T. Akiyama, *Chem. Rev.* **2007**, *107*, 5744–5758.
[4] T. Akiyama, K. Mori, *Chem. Rev.* **2015**, *115*, 9277–9306.
[5] M. Mahlau, B. List, *Angew. Chem. Int. Ed.* **2013**, *52*, 518–533.
[6] T. Akiyama, J. Itoh, K. Yokota, K. Fuchibe, *Angew. Chem. Int. Ed.* **2004**, *43*, 1566–1568.
[7] D. Uraguchi, M. Terada, *J. Am. Chem. Soc.* **2004**, *126*, 5356–5357.
[8] S. Hoffmann, A. M. Seayad, B. List, *Angew. Chem. Int. Ed.* **2005**, *44*, 7424–7427.
[9] R. I. Storer, D. E. Carrera, Y. Ni, D. W. C. MacMillan, *J. Am. Chem. Soc.* **2006**, *128*, 84–86.
[10] M. Rueping, E. Sugiono, C. Azap, T. Theissmann, M. Bolte, *Org. Lett.* **2005**, *7*, 3781–3783.
[11] M. Sickert, F. Abels, M. Lang, J. Sieler, C. Birkemeyer, C. Schneider, *Chem. Eur. J.* **2010**, *16*, 2806–2818.
[12] Q. X. Guo, H. Liu, C. Guo, S. W. Luo, Y. Gu, L. Z. Gong, *J. Am. Chem. Soc.* **2007**, *129*, 3790–3791.
[13] D. Uraguchi, K. Sorimachi, M. Terada, *J. Am. Chem. Soc.* **2004**, *126*, 11804–11805.
[14] G. B. Rowland, E. B. Rowland, Y. Liang, J. A. Perman, J. C. Antilla, *Org. Lett.* **2007**, *9*, 2609–2611.
[15] M. Rueping, A. P. Antonchick, T. Theissmann, *Angew. Chem. Int. Ed.* **2006**, *45*, 6751–6755.

Angew. Chem. Int. Ed. **2023**, *62*, e202301183 (8 of 9)

© 2023 The Authors. Angewandte Chemie International Edition published by Wiley-VCH GmbH

[16] P. Jiao, D. Nakashima, H. Yamamoto, *Angew. Chem. Int. Ed.* **2008**, *47*, 2411–2413.

[17] Q. Yin, S. G. Wang, S. L. You, *Org. Lett.* **2013**, *15*, 2688–2691.

[18] M. Rueping, T. Theissmann, M. Stoeckel, A. P. Antonchick, *Org. Biomol. Chem.* **2011**, *9*, 6844–6850.

[19] M. Yamanaka, J. Itoh, K. Fuchibe, T. Akiyama, *J. Am. Chem. Soc.* **2007**, *129*, 6756–6764.

[20] P. Renzi, J. Hioe, R. M. Gschwind, *J. Am. Chem. Soc.* **2017**, *139*, 6752–6760.

[21] M. Melikian, J. Gramüller, J. Hioe, J. Greindl, R. M. Gschwind, *Chem. Sci.* **2019**, *10*, 5226–5234.

[22] J. Greindl, J. Hioe, N. Sorgenfrei, F. Morana, R. M. Gschwind, *J. Am. Chem. Soc.* **2016**, *138*, 15965–15971.

[23] M. Žabka, R. M. Gschwind, *Chem. Sci.* **2021**, *12*, 15263–15272.

[24] N. Sorgenfrei, J. Hioe, J. Greindl, K. Rothermel, F. Morana, N. Lokesh, R. M. Gschwind, *J. Am. Chem. Soc.* **2016**, *138*, 16345–16354.

[25] K. Rothermel, M. Melikian, J. Hioe, J. Greindl, J. Gramüller, M. Žabka, N. Sorgenfrei, T. Hausler, F. Morana, R. M. Gschwind, *Chem. Sci.* **2019**, *10*, 10025–10034.

[26] D. Jansen, J. Gramüller, F. Niemeyer, T. Schaller, M. C. Letzel, S. Grimme, H. Zhu, R. M. Gschwind, J. Niemeyer, *Chem. Sci.* **2020**, *11*, 4381–4390.

[27] J. Gramüller, M. Franta, R. M. Gschwind, *J. Am. Chem. Soc.* **2022**, *144*, 19861–19871.

[28] L. Simón, J. M. Goodman, *J. Am. Chem. Soc.* **2008**, *130*, 8741–8747.

[29] T. Marcelli, P. Hammar, F. Himo, *Chem. Eur. J.* **2008**, *14*, 8562–8571.

[30] J. P. Reid, J. M. Goodman, *J. Am. Chem. Soc.* **2016**, *138*, 7910–7917.

[31] J. P. Reid, J. M. Goodman, *Chem. Eur. J.* **2017**, *23*, 14248–14260.

[32] J. P. Reid, M. S. Sigman, *Nature* **2019**, *571*, 343–348.

[33] A. J. Neel, A. Milo, M. S. Sigman, F. D. Toste, *J. Am. Chem. Soc.* **2016**, *138*, 3863–3875.

[34] M. Orlandi, J. A. S. Coelho, M. J. Hilton, F. D. Toste, M. S. Sigman, *J. Am. Chem. Soc.* **2017**, *139*, 6803–6806.

[35] R. Maji, S. C. Mallojjala, S. E. Wheeler, *Chem. Soc. Rev.* **2018**, *47*, 1142–1158.

[36] K. Kaupmees, N. Tolstoluzhsky, S. Raja, M. Rueping, I. Leito, *Angew. Chem. Int. Ed.* **2013**, *52*, 11569–11572.

[37] R. Mitra, H. Zhu, S. Grimme, J. Niemeyer, *Angew. Chem. Int. Ed.* **2017**, *56*, 11456–11459.

[38] M. Rueping, C. Azap, E. Sugiono, T. Theissmann, *Synlett* **2005**, 2367–2369.

[39] S. G. Ouellet, A. M. Walji, D. W. C. Macmillan, *Acc. Chem. Res.* **2007**, *40*, 1327–1339.

[40] Despite the increased polarity of CD_2Cl_2 compared with toluene, e.g. large ion pair aggregates were found to dominate the reactivity of a photocatalytic reaction in this solvent see e.g. N. Berg, S. Bergwinkl, P. Nuernberger, D. Horinek, R. M. Gschwind, *J. Am. Chem. Soc.* **2021**, *143*, 724–735.

[41] N. Lokesh, J. Hioe, J. Gramüller, R. M. Gschwind, *J. Am. Chem. Soc.* **2019**, *141*, 16398–16407.

[42] S. Sharif, G. S. Denisov, M. D. Toney, H. H. Limbach, *J. Am. Chem. Soc.* **2007**, *129*, 6313–6327.

[43] P. Schah-Mohammedi, I. G. Shenderovich, C. Detering, H. H. Limbach, P. M. Tolstoy, S. N. Smirnov, G. S. Denisov, N. S. Golubev, *J. Am. Chem. Soc.* **2000**, *122*, 12878–12879.

[44] C. Detering, P. M. Tolstoj, N. S. Golubev, G. S. Denisov, H. H. Lumbach, *Dokl. Akad. Nauk* **2001**, *379*, 353–357.

[45] L. Schreyer, R. Properzi, B. List, *Angew. Chem. Int. Ed.* **2019**, *58*, 12761–12777.

[46] X. H. Chen, W. Q. Zhang, L. Z. Gong, *J. Am. Chem. Soc.* **2008**, *130*, 5652–5653.

[47] H. Yamamoto, K. Futatsugi, *Angew. Chem. Int. Ed.* **2005**, *44*, 1924–1942.

[48] R. Zhao, L. Shi, *ChemCatChem* **2014**, *6*, 3309–3311.

[49] V. H. Rawal, A. N. Thadani, A. K. Unni, Y. Huang, *Nature* **2003**, *424*, 146.

[50] N. T. Mcdougal, S. E. Schaus, *J. Am. Chem. Soc.* **2003**, *125*, 12094–12095.

[51] T. Hashimoto, K. Maruoka, *J. Am. Chem. Soc.* **2007**, *129*, 10054–10055.

[52] R. Davydov, S. Chemerisov, D. E. Werst, T. Rajh, T. Matsui, M. Ikeda-Saito, B. M. Hoffman, *J. Am. Chem. Soc.* **2004**, *126*, 15960–15961.

[53] G. Dodson, A. Wlodawer, *Trends Biochem. Sci.* **1998**, *23*, 347–352.